



# High-resolution carbon isotopic records from the Ordovician of South China: Links to climatic cooling and the Great Ordovician Biodiversification Event (GOBE)

Tonggang Zhang<sup>a</sup>, Yanan Shen<sup>a,\*</sup>, Thomas J. Algeo<sup>b</sup>

<sup>a</sup> Biogeochemistry and Paleoenvironment Research Group & LPS, Nanjing Institute of Geology and Palaeontology, Chinese Academy of Sciences, Nanjing 210008, China

<sup>b</sup> Department of Geology, University of Cincinnati, Cincinnati, OH 45221-0013 USA

## ARTICLE INFO

### Article history:

Received 13 August 2009

Received in revised form 3 February 2010

Accepted 18 February 2010

Available online 24 February 2010

### Keywords:

$\delta^{13}\text{C}_{\text{carb}}$

$\delta^{13}\text{C}_{\text{org}}$

Atmospheric  $\text{CO}_2$

Climate cooling

Biodiversification

## ABSTRACT

The Great Ordovician Biodiversification Event (GOBE) represented the largest increase in diversity in the marine biosphere during the Phanerozoic Eon, yet its causes and consequences remain poorly understood. Patterns of isotopic variation in high-resolution  $\delta^{13}\text{C}_{\text{carb}}$  and  $\delta^{13}\text{C}_{\text{org}}$  records from a well-exposed section at Honghuayuan in South China may provide important insights regarding the GOBE. The Honghuayuan isotopic profiles, which can be correlated with C-isotopic records from contemporaneous sections globally, reveal large perturbations to the global carbon cycle during the Ordovician. A +8‰ increase in  $\delta^{13}\text{C}_{\text{org}}$  values in the Floian implies a large, albeit transient increase in the burial rate of organic matter during the mid-Early Ordovician that may have contributed to climatic cooling and played an important role in triggering the GOBE. A +4‰ increase in  $\delta^{13}\text{C}_{\text{carb}}$  and high-frequency variation in  $\delta^{13}\text{C}_{\text{org}}$  in the Darriwilian to Sandbian suggest a second episode of elevated organic carbon burial rates accompanied by substantial instability in the global carbon cycle during the late Middle and early Late Ordovician. This pattern may mark the onset of climate changes culminating in the end-Ordovician Hirnantian glaciation and mass extinction event that terminated the GOBE.

© 2010 Elsevier B.V. All rights reserved.

## 1. Introduction

The “Great Ordovician Biodiversification Event” (GOBE) began ~470 Ma ago during the Early Ordovician and possibly lasted more than 25 Myr into the Late Ordovician (Droser and Sheehan, 1997; Miller, 1997; Webby et al., 2004; Servais et al., 2009). Whereas the Cambrian explosion resulted in the appearance of nearly all phyla of marine animals, biodiversity at the taxonomic ranks of family, genus and species remained low until the Ordovician (Sepkoski, 1997). By the end of the Ordovician, biodiversity at the family level had increased to more than three times that in the Cambrian and Early Ordovician (Webby et al., 2004). The GOBE was terminated by a major mass extinction at the end of the Ordovician, ~444 Ma ago (Sepkoski, 1996; timescale of Gradstein et al., 2004), which may have been triggered by climatic cooling culminating in the Hirnantian (latest Ordovician) glaciation (Stanley, 1984; Sheehan, 2001), during which icesheets spread across much of Gondwana and part of Laurentia (Crowell, 1999).

Relative to the Cambrian explosion and end-Ordovician mass extinction, the GOBE has received less attention (Bottjer et al., 2001), and the cause of this event remains debated (Servais et al., 2009). It was traditionally proposed that the GOBE did not coincide with any abrupt environmental changes, and that it simply represented a realization of innate

evolutionary potential among early metazoans (Webby et al., 2004). However, recent studies have emphasized the role of environmental changes as a trigger for the GOBE. Trotter et al. (2008) argued on the basis of oxygen-isotopic thermometry of conodonts that climatic cooling may have led to the GOBE. Alternatively, Schmitz et al. (2008) suggested on the basis of changes in the abundance of extraterrestrial chromite grains and the ratio of seawater  $^{187}\text{Os}/^{188}\text{Os}$  that meteorite impacts accelerated the pace of biodiversification during the Early to Middle Ordovician.

Warm global climatic conditions have been inferred for the Early to Middle Ordovician on the basis of atmospheric  $\text{pCO}_2$  levels that are estimated to have been 14 to 18 times the present atmospheric level (Bernier and Kothavala, 2001; Herrmann et al., 2003). Therefore, it has been widely assumed that the GOBE may have occurred during a period of greenhouse conditions (e.g., Gibbs et al., 1997). However, both the onset and termination of this greenhouse period are poorly constrained (Saltzman and Young, 2005), so its temporal relationship to the GOBE remains unclear. Because atmospheric  $\text{CO}_2$  is an important greenhouse gas in the atmosphere, variations thereof are commonly suggested to be the main driver of climate change on geological timescales ( $>10^6$  yr), and at intermediate timescales ( $10^3$ – $10^6$  yr), atmospheric  $\text{pCO}_2$  is controlled by the input and removal of carbon to the ocean-atmosphere system (e.g., Royer, 2006). Therefore, the carbon isotopic compositions of carbonate and organic carbon have the potential to record changes in the global carbon cycle that may have been associated with changes in atmospheric  $\text{pCO}_2$  (Hayes et al., 1999; Kump and Arthur, 1999; Freeman, 2001).

\* Corresponding author.

E-mail address: [yshen@nigpas.ac.cn](mailto:yshen@nigpas.ac.cn) (Y. Shen).

A great number of studies have constructed C-isotopic chemostratigraphic profiles for portions of the Ordovician–Silurian in sections with a global distribution (Wang et al., 1993a; Patzkowsky et al., 1997; Underwood et al., 1997; Kump et al., 1999; Finney et al., 1999; Brenchley et al., 2003; Buggisch et al., 2003; Shields et al., 2003; Saltzman, 2005; Saltzman and Young 2005; Melchin and Holmden, 2006; Kaljo et al., 2007), including sections in South China (Wang et al., 1993b, 1997; Chen et al., 2006a; Zhang et al., 2009; Fan et al., 2009; Yan et al., 2009; Bergström et al., 2009). Although such records have improved global correlations of Ordovician–Silurian strata (e.g., Sheehan, 2001), most of the sections utilized represent relatively short stratigraphic intervals. In this study, we report high-resolution records for organic carbon ( $\delta^{13}\text{C}_{\text{org}}$ ) and carbonate carbon ( $\delta^{13}\text{C}_{\text{carb}}$ ) isotopes from a well-exposed section at Honghuayuan in South China that spans nearly the entire Ordovician. These records exhibit characteristic features that may help to refine the timing of termination of the Cambrian–Ordovician greenhouse climate and that provide insights into relationships between concurrent changes in climate and biodiversity during the Ordovician.

## 2. Geology setting and stratigraphy

### 2.1. Regional geology

During the Ordovician, the China Block consisted of four separate cratons: North China, South China, Tarim, and Chaidam–Tibet (Wang, 1985). On the South China craton, which was covered by a broad epeiric sea, continuous and richly fossiliferous Ordovician–Silurian sequences were widely developed (Chen et al., 2004). By the Late Ordovician, the South China craton had separated from the Gondwanan supercontinent, and it was located at a paleolatitude of about 20°S (e.g., Chen et al., 2004).

During the past several decades, the lithostratigraphy, biostratigraphy, and sedimentary environments of numerous Ordovician sections in South China have been extensively investigated (Mu et al., 1981; Rong and Harper, 1988; Wang and Chen, 1991; Rong et al., 2002; Chen et al., 2004, 2005; 2006a, b; Zhan et al., 2007; Zhan and Jin,

2007, 2008; Hu et al., 2008). Three of these sections were selected as Global Stratotype Sections and Points (GSSPs) for the base of Dapingian, the base of Darriwilian, and the base of Hirnantian owing to their rich fossil records, especially of graptolites and conodonts that are of great utility for global correlations (Chen et al., 2006a; Zhan and Jin, 2008).

Our samples were collected from the Honghuayuan section located at N28°4'31", E106°51'45", about 7 km southeast of Tongzi county, in northern Guizhou Province, China (Fig. 1). The Honghuayuan section represents a stratigraphically continuous and richly fossiliferous succession extending from the Upper Cambrian to the Lower Silurian. This section has been studied for over 50 years, and the lithostratigraphy, biostratigraphy, and chronology of the section are well established (Chen et al., 2000; Rong et al., 2002; Zhan and Jin, 2007 and references therein). Paleontological research at Honghuayuan has documented in detail the pattern of biodiversification and mass extinction during the Ordovician, and these observations can be correlated with data from the GSSP section at Wangjiawan in Yichang (Fig. 1, Chen et al., 2006a). These earlier studies provide the framework within which we have generated new, high-resolution C-isotope record at Honghuayuan for studying the relationship between Ordovician bioevents and major changes in the carbon cycle.

### 2.2. Lithostratigraphy and biostratigraphy at Honghuayuan

At Honghuayuan, the base of the Ordovician section is conformable with underlying carbonates of the Upper Cambrian Loushankuan Group, and the top of the section is conformable with shales of the Lower Silurian Lungmachi Formation. Ordovician strata are subdivided, in ascending order, into the Tungtzu, Hunghuayuan, Meitan, Shihtzupu, Pagoda, Linhsiang, Wufeng, and Kuanyinchiao formations (Fig. 2). The Tungtzu, Hunghuayuan, and lower Meitan formations comprise the Lower Ordovician, the upper Meitan and Shihtzupu formations comprise the Middle Ordovician, and the Pagoda, Linhsiang, Wufeng, and Kuanyinchiao formations comprise the Upper Ordovician (e.g., Zhan and Jin, 2007). With the exception of the Tungtzu Formation, which was mostly covered, these strata are continuously

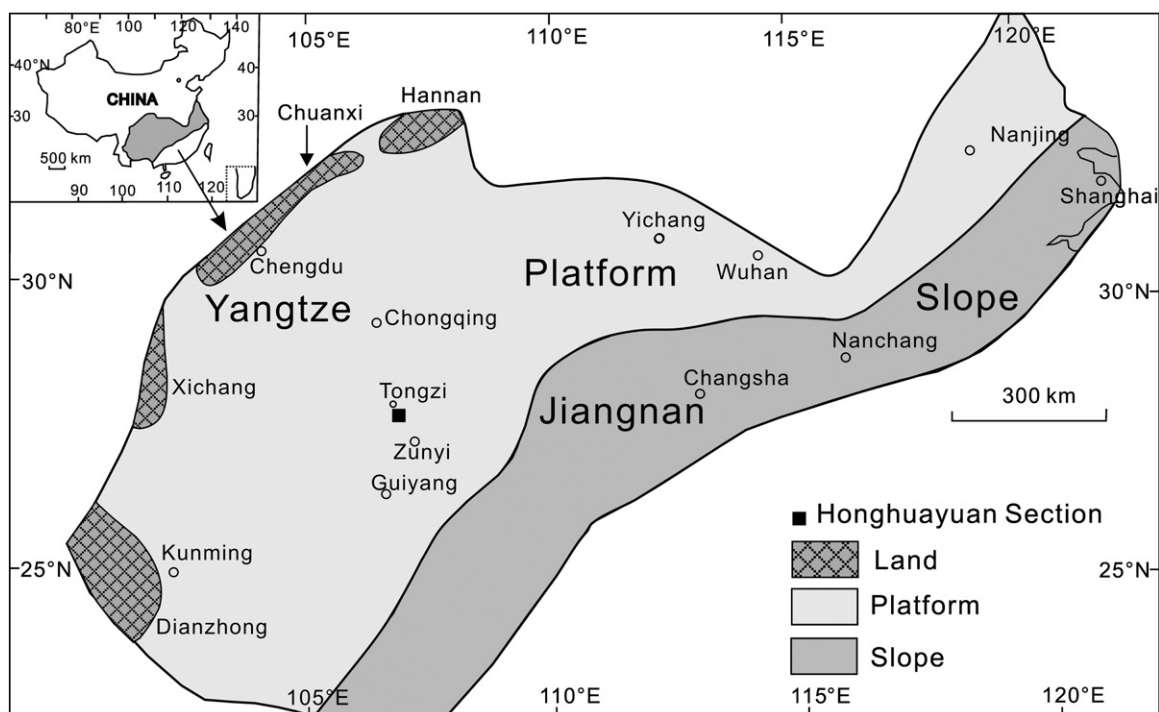


Fig. 1. Location and paleogeography map for the Honghuayuan section in South China (modified from Zhan and Jin, 2007).

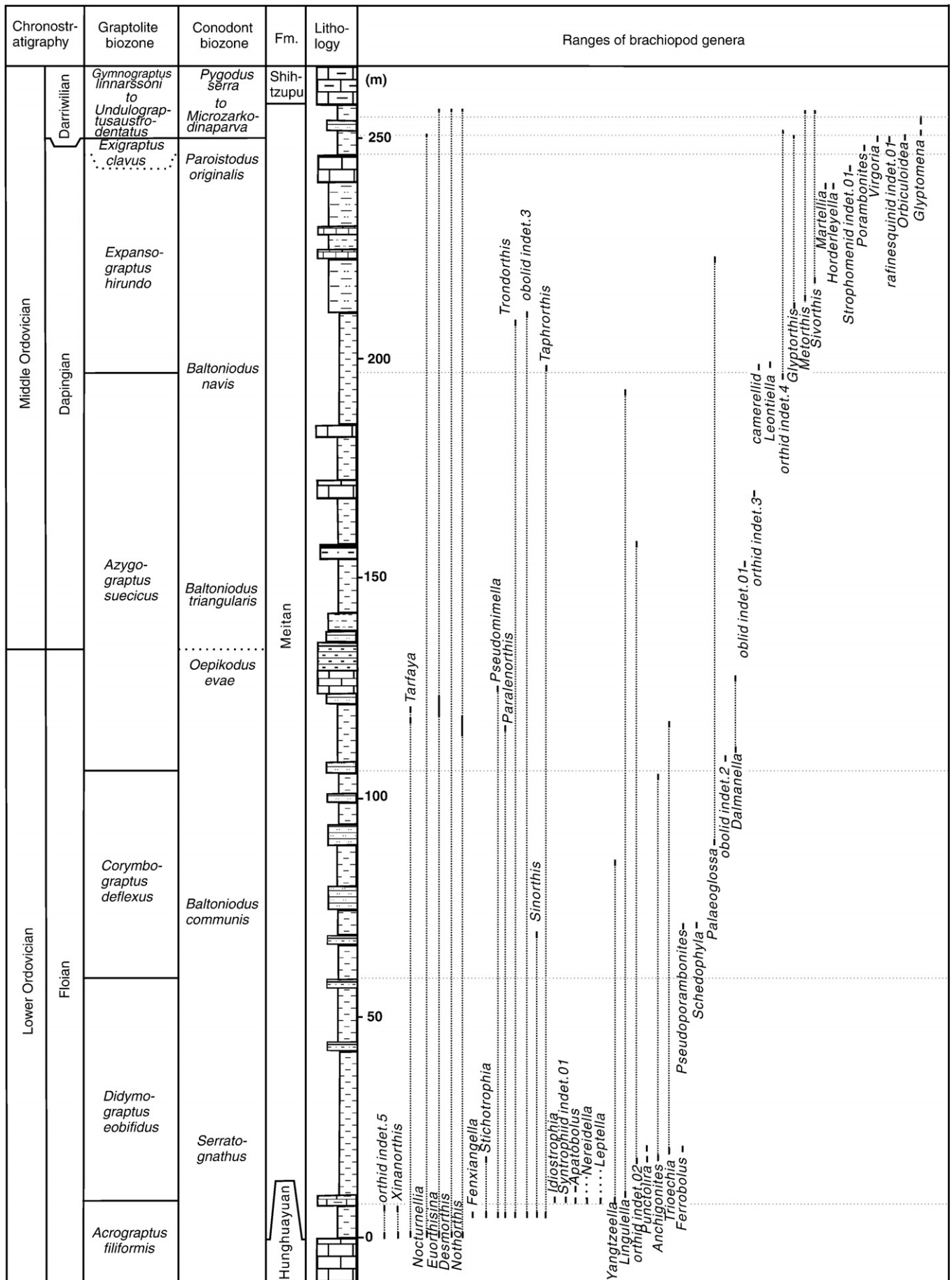


Fig. 2. Brachiopod radiation in Early to Middle Ordovician at Honghuayuan in South China (modified from Zhan et al. 2005).

exposed along a mountainside at Honghuayuan. The detailed litho- and biostratigraphy of the Honghuayuan section were reported by Zhan and Jin (2007). It should be pointed out that biostratigraphy and fossil assemblages as well as divisions of bizones for the Honghuayuan section in our study were established by previous investigations (Zhan and Jin, 2007 and references therein). A brief description of the six main stratigraphic units at Honghuayuan, from oldest to youngest, follows:

- (1) The Tungtzu Formation (Tremadocian) is 105.4 m thick and consists of gray, thin- to medium-bedded micritic dolostone, bioclastic limestone, oolitic limestone, including a few yellowish green shale interlayers. The bioclastic limestones contain the trilobites *Asaphellus*, *Dactylocephalus*, *Asaphopsis*, *Wanliangtingia*, *Psilocephalina*, *Tungtzuella* (Fu, 1982), and the brachiopods *Apheoorthis*, *Imbriacatia*, *Lingulella*, *Syntrophina*, *Hesperonomia* (Chen et al., 1995).
- (2) The Hunghuayuan Formation (basal Floian) is 34.2 m thick and consists of gray to dark gray, medium- to thick-bedded limestones with a single 2-m-thick shale interbed. The bioclastic limestones contain abundant trilobites (e.g., *Liomegalaspides*, *Psilocephalina*), and brachiopods (e.g., *Trematorthis*, *Hesperonomia*, *Apheoorthis*, *Tritoechia*) (Chen et al., 1995), and conodonts, whereas the shale yielded abundant graptolites (e.g., *Acrograptus saukros*, *Corymbograptus cf. vacillans*) (Chen et al., 1995; Zhang and Chen, 2003).
- (3) The Meitan Formation has a total thickness of ~258 m and is subdivided into lower (Floian) and upper (Dapingian) parts at the base of a limestone bed located ~120 m above the base of the formation. The lower part consists of yellowish green fossil-rich mudstones interbedded with siltstones, and the upper part contains relatively more siltstones and fossil-rich limestones. Brachiopods, the single most abundant fossil group, form several distinct communities, including the Paralenorthis, Sinorthis, and Desmorthis communities, in the lower Meitan. In the upper Meitan, various short-lived brachiopod associations are dominated by opportunistic taxa such as *Methorthis*, *Lepidorthis*, *Virgoria*, and *Martellia*. Graptolites are the second most abundant fossil group, allowing subdivision of the formation into eight graptolite biozones (Fig. 2; Zhang and Chen, 2003). Trilobites are more variable in occurrence but relatively less abundant than brachiopods and graptolites.
- (4) The Shihtzupu Formation (Darriwilian) is 9.3 m thick and characterized by lithologically distinct lower and upper parts.
- (5) The Pagoda Formation (Sandbian to lower Katian; = Caradoc) is 36.9 m thick and consists of light gray, medium- to thick-bedded micritic limestones. It is moderately rich in fossils such as trilobites, nautiloids, and brachiopods. Nautiloids are the most important fauna in this formation, especially *Sinoceras chinense* and *Michelinoceras sp.* (Chen et al., 1995). Trilobites and brachiopods, often of diminutive size, are also abundant (Rong et al., 1999).
- (6) The Linhsiang Formation (middle Katian) is 4.3 m thick and consists of light gray, argillaceous nodular-like limestones and dark gray, calcareous mudstones. Trilobites and brachiopods are found in the limestones, and graptolites, especially *Dicellograptus complanatus*, *Amplexograptus latus*, *Climacograptus sp.*, and *Leptograptus sp.*, are the most abundant fossils in the mudstone beds (Chen et al., 2000).

### 2.3. Ordovician radiation in South China

The GOBE is reflected in diversifications within many marine invertebrate clades during the Early to Middle Ordovician. Though GOBE generated few higher taxa, it did produce a staggering increase in biodiversity at the family, genus and species levels (Webby et al., 2004). As such, in terms of taxonomic terms, GOBE may record the greatest interval of biodiversification of life over the last 3.8 billion years.

The Honghuayuan section preserves one of the best records of the GOBE in South China. Detailed paleontological investigations revealed macroevolutionary patterns of marine animals of different ecotypes during the diversification event (e.g., Zhan et al., 2005). At Honghuayuan, the Early Ordovician radiation resulted in a small increase in the number of brachiopod orders and a larger increase in the number of families (from 6 to 24) and genera (from 8 to 57) (Zhan and Jin, 2007). The diversification began slowly within the *Tetragraptus* biozone of the Tremadocian and accelerated within the *Acrograptus*

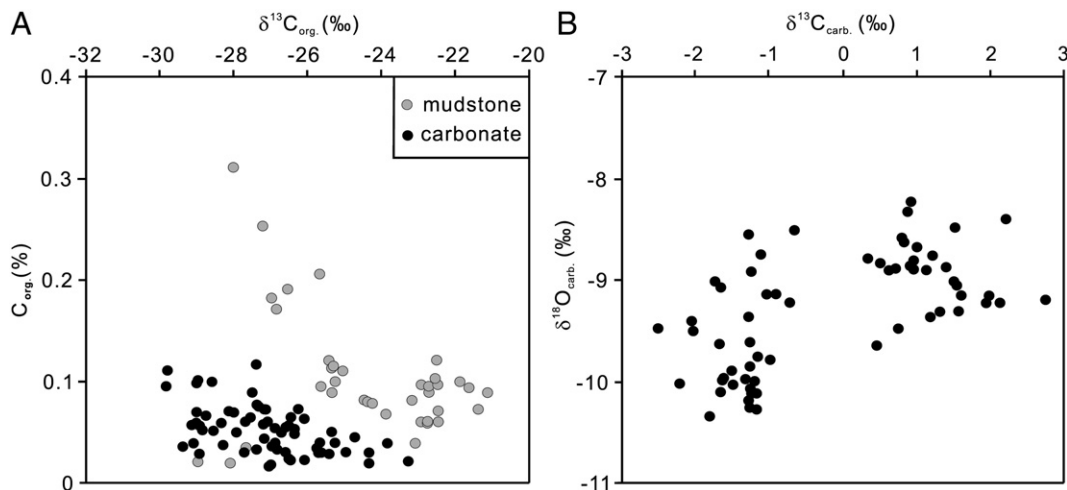


Fig. 3. Evaluation of the diagenetic influence on C-isotope compositions: (A)  $\delta^{13}C_{org}$  versus  $C_{org}$ ; (B)  $\delta^{13}C_{carb}$  versus  $\delta^{18}O_{carb}$ .

*filiformis* Biozone at the base of the Meitan Formation (Fig. 2). Brachiopod biodiversity reached its first peak within the *Didymograptus eobifidus* Biozone of the lower Meitan Formation, about four graptolite biozones earlier than in North America and in Baltic (Zhan and Jin, 2007, 2008) (Fig. 2). Brachiopods underwent not only a sharp increase in taxonomic abundance but also a dramatic change in the range of habitats occupied and ecological roles played (e.g., Zhan and Jin, 2007). In terms of biodiversity and ecological dominance, orthids and pentamerids became the most important orders of brachiopods at this time (Zhan et al., 2005; Zhan and Harper, 2006).

### 3. Sample collection and analytical methods

Carbonate and shale samples were collected for carbon isotopic analysis. After washing and cutting to remove weathered parts, each sample was crushed and milled to a uniform powder in an automated agate mortar device. For organic carbon analysis, about 2 g of powdered sample were treated with 6 N HCl for 24 h to remove carbonate minerals, followed by washing and filtering of the residue. The residue was then dried and weighed prior to organic carbon isotope analysis. Organic carbon contents were determined using a NC Instruments NC 2500<sup>TM</sup> elemental analyzer. Organic carbon isotopic compositions were determined using a VG Micromass Isoprime<sup>TM</sup> mass spectrometer coupled to an Elementar Vario Micro Cube<sup>TM</sup> elemental analyzer with continuous flow. Based on the predetermined organic carbon concentration, from 100 µg to 10 mg samples were weighed and combusted in the elemental analyzer, and the pure CO<sub>2</sub> gas was sent to the mass spectrometer for <sup>13</sup>C/<sup>12</sup>C determination. Analytical reproducibility was approximately 0.1‰ based on analysis of IAEA standards.

Carbon isotopic compositions of carbonate samples were determined by a traditional acid-release method. Powdered samples were treated with anhydrous H<sub>3</sub>PO<sub>4</sub> at 25 °C for 24 h to liberate CO<sub>2</sub>, and the purified CO<sub>2</sub> was sealed for carbon isotope analysis. The carbon isotopic ratio was analyzed on a Finnigan MAT 252 mass spectrometer. Results are reported in standard per mil δ-notation relative to the V-PDB standard. Analytical precision of these analyses is better than 0.1‰. Geochemical data (TOC, δ<sup>13</sup>C<sub>org</sub> and δ<sup>13</sup>C<sub>carb</sub>) are given in Table 1.

## 4. Results and discussion

### 4.1. Evaluation of secondary effects on isotopic records at Honghuayuan

The C isotopic signature of organic matter (δ<sup>13</sup>C<sub>org</sub>) is potentially influenced by a number of environmental and diagenetic factors. Where the isotopic composition of bulk organic matter is analyzed (as in the present study), admixture of terrestrial organic matter can result in δ<sup>13</sup>C<sub>org</sub> values that deviate from those of pure marine organic matter to varying degrees (e.g., Cramer and Saltzman, 2007). However, the influence of terrestrial organic carbon input on the δ<sup>13</sup>C<sub>org</sub> values of Ordovician samples was limited at most owing to an absence of higher land plants at that time (Selden and Edwards, 1989). Bryophytes were present but probably in low abundance and their non-woody tissues probably decayed rapidly, leading to little contribution to bulk organic matter in contemporaneous marine sediments.

Bacterial and thermogenic destruction of specific fractions of organic matter during early to late diagenesis can lead to a shift in the C-isotopic composition of bulk organic matter (Freeman, 2001). Recrystallization plays an important role in the preservation of organic matter in carbonate sediments (Ingalls et al., 2004). Organic matter that enters the oil window generally yields <sup>12</sup>C-enriched hydrocarbons, so the isotopic composition of the residual kerogen becomes enriched in <sup>13</sup>C (Hayes et al., 1989). The degree of thermal maturation of the sediment thus influences its bulk organic δ<sup>13</sup>C composition. For the study units, there are several important considerations regarding the potential effects of

thermal alteration. First, Ordovician sedimentary rocks in South China are relatively immature thermally, as shown by low conodont colour alteration indices (CAI = 2.0–2.5) and low vitrinite reflectance (R<sub>0</sub>) for graptolites (1.0–1.1%), chitinozoans (1.28), scolecodonts (1.04–1.23), bitumen (1.0–1.22), and kerogen (0.9) (Wang et al., 1993). Second, although systematic correlation between δ<sup>13</sup>C<sub>org</sub> and organic carbon content (C<sub>org</sub>) may develop through diagenesis (e.g., Kump et al., 1999; Shen and Schidlowski, 2000), no systematic relationship was observed between δ<sup>13</sup>C<sub>org</sub> and organic carbon content (C<sub>org</sub>) at either the biozone or formation level in the Honghuayuan section (Fig. 3A). These observations suggest at most limited diagenetic alteration of primary marine organic δ<sup>13</sup>C values in the Honghuayuan section.

The C isotopic compositions of carbonates can also potentially be altered through diagenetic reactions, especially at high water/rock ratios (>~20) or where inorganic carbon sources with markedly different isotopic compositions (e.g., DIC produced through oxidation of methane) are present in sediment porewaters. Water/rock ratios in the diagenetic environment of the study section can be estimated from O-isotopic ratios and burial temperatures. Most δ<sup>18</sup>O<sub>carb</sub> values at Honghuayuan are between –8‰ and –10‰ (Table 1), which are equivalent to water/rock ratios of 3–10 (Algeo et al., 1992) at burial temperatures of 60–80 °C (Wang et al., 1993). The Honghuayuan section exhibits only a limited range of δ<sup>13</sup>C<sub>carb</sub> values (–2‰ to +4‰), which is consistent with a primary marine signature and with estimates of low diagenetic water/rock ratios. A lack of systematic correlation between δ<sup>13</sup>C<sub>carb</sub> and δ<sup>18</sup>O<sub>carb</sub> at either the biozone or formation level in the studied section (Fig. 3B) provides further evidence of only minimal secondary alteration of the carbonate C-isotopic record at Honghuayuan. On the other hand, the O-isotopic composition of carbonates is commonly altered at water/rock ratios as low as 1–3 (Algeo et al., 1992), and the range of δ<sup>18</sup>O<sub>carb</sub> values observed at Honghuayuan (–8‰ and –10‰; Fig. 3B) implies at least a modest negative shift from contemporaneous primary marine values (Lohmann and Walker, 1989). Thus, most of the carbonate O-isotopic record at Honghuayuan can be regarded as of secondary origin.

### 4.2. C-isotopic chemostratigraphy of the Honghuayuan section

The organic C-isotope chemostratigraphy for Honghuayuan shows several remarkable changes from the middle Floian to the lower Katian (Fig. 4B). At Honghuayuan, the first large shift of δ<sup>13</sup>C<sub>org</sub> occurred in the Floian stage. From the middle of the *Acrograptus filiformis* biozone to the top of the *Didymograptus eobifidus* biozone, δ<sup>13</sup>C<sub>org</sub> values rise from –29.4‰ to –21.1‰, then δ<sup>13</sup>C<sub>org</sub> values show a decreased trend from –21.1‰ to –27.2‰ towards the top of the *Azygograptus suecicus* biozone of the Dapingian stage. It is evident that δ<sup>13</sup>C<sub>org</sub> exhibits an increase of ~8‰ in the Floian stage at Honghuayuan (Fig. 4B). The Middle and Upper Ordovician also exhibit significant variation in δ<sup>13</sup>C<sub>org</sub> values: the Dapingian through Katian stages show several large (~4‰) fluctuations, accompanied by a shift in average δ<sup>13</sup>C<sub>org</sub> values of ~–26.5‰ in the Dapingian to ~–29‰ in the upper Katian (Fig. 4B).

The carbonate C-isotope chemostratigraphy for Honghuayuan also shows a few major features (Figs. 4A, 5A). δ<sup>13</sup>C<sub>carb</sub> values rise from –1.1‰ to +1.5‰, and exhibit a ~3‰ positive increase from the upper part of carbonate sequence of the Meitan Formation to the lower part of the Shihtzupu Formation. This δ<sup>13</sup>C<sub>carb</sub> increase is followed by a ~1.5‰ decrease towards the topmost of the Shihtzupu Formation. Biostratigraphically, the δ<sup>13</sup>C<sub>carb</sub> increase of ~3‰ and subsequent decrease of ~1.5‰ from the top of the Meitan to the topmost of the Shihtzupu Formation occur in the Darrivilian Stage. A second large δ<sup>13</sup>C<sub>carb</sub> rise, from +0.3‰ to +2.7‰, is observed from the topmost of the Shihtzupu Formation to the lowermost Pagoda Formation of the early Sandbian (Fig. 5A). Within most of the Pagoda Formation (i.e., from Sandbian to middle Katian), δ<sup>13</sup>C<sub>carb</sub> values vary between +1‰ and +2‰ and show little stratigraphic change.

Table 1

Sample	Formation	Lithology	Depth (m)	$\delta^{13}\text{C}_{\text{org}}$	Corg (%)	$\delta^{13}\text{C}_{\text{carb}}$	$\delta^{18}\text{O}_{\text{carb}}$
GZ04	Hunghuayuan	Carbonate	0.50	-29.08	0.04	-1.02	-9.14
GZ05	Hunghuayuan	Carbonate	1.50	-28.52	0.05	-1.25	-8.92
GZ06	Hunghuayuan	Carbonate	3.00	-28.85	0.05	-1.64	-9.07
GZ07	Hunghuayuan	Carbonate	5.00	-29.12	0.06	-2.05	-9.40
GZ08	Hunghuayuan	Carbonate	7.50	-29.01	0.06	-1.67	-9.63
GZ09	Hunghuayuan	Carbonate	12.81	-29.36	0.04	-1.50	-9.89
GZ10	Hunghuayuan	Carbonate	15.00	-27.68	0.06	-1.31	-9.98
GZ11	Hunghuayuan	Carbonate	16.00	-24.96	0.03	-1.60	-9.96
GZ12	Hunghuayuan	Carbonate	17.50	-28.27	0.04	-1.62	-9.99
GZ13	Hunghuayuan	Carbonate	20.00	-28.92	0.03	-1.25	-9.62
GZ14	Hunghuayuan	Carbonate	22.41	-27.53	0.07	-1.23	-10.12
GZ15	Hunghuayuan	Carbonate	24.55	-28.32	0.06	-1.25	-10.06
GZ16	Hunghuayuan	Carbonate	27.75	-27.13	0.07	-1.28	-9.37
GZ17	Hunghuayuan	Carbonate	30.74	-27.38	0.03	-1.20	-9.99
GZ18	Hunghuayuan	Carbonate	32.87	-25.42	0.03	-1.27	-8.55
GZ19	Hunghuayuan	Carbonate	33.30	-26.81	0.03	-1.73	-9.02
GZ20	Hunghuayuan	Carbonate	33.72	-27.04	0.02	-2.03	-9.50
GZ21	Hunghuayuan	Carbonate	34.15	-26.45	0.02	-2.21	-10.02
GZ23	Meitan	Carbonate	35.27	-26.50	0.02	-1.65	-10.10
GZ26	Meitan	Carbonate	42.73	-24.34	0.02	-2.51	-9.47
GZ27	Meitan	Carbonate	43.33	-26.57	0.03	-1.48	-10.03
GZ159	Meitan	mudstone	48.53	-23.16	0.08		
GZ160	Meitan	mudstone	53.59	-22.92	0.10		
GZ161	Meitan	Mudstone	57.63	-22.45	0.07		
GZ162	Meitan	Mudstone	62.71	-22.71	0.10		
GZ163	Meitan	Mudstone	67.73	-22.45	0.10		
GZ164	Meitan	Mudstone	72.81	-22.53	0.10		
GZ165	Meitan	Mudstone	77.87	-21.63	0.09		
GZ166	Meitan	Mudstone	85.93	-21.37	0.07		
GZ167	Meitan	Mudstone	92.01	-21.12	0.09		
GZ168	Meitan	Mudstone	100.93	-22.71	0.09		
GZ169	Meitan	Mudstone	107.39	-22.50	0.12		
GZ170	Meitan	Mudstone	115.92	-22.44	0.06		
GZ171	Meitan	Mudstone	120.51	-22.75	0.06		
GZ172	Meitan	Mudstone	125.04	-22.93	0.06		
GZ173	Meitan	Mudstone	132.50	-23.88	0.07		
GZ174	Meitan	Mudstone	137.16	-24.40	0.08		
GZ175	Meitan	Mudstone	142.69	-24.48	0.08		
GZ176	Meitan	Mudstone	147.21	-24.26	0.08		
GZ177	Meitan	Mudstone	149.03	-22.74	0.06		
GZ178	Meitan	Mudstone	150.50	-21.86	0.10		
GZ179	Meitan	Mudstone	152.07	-25.32	0.09		
GZ180	Meitan	Mudstone	155.09	-25.62	0.10		
GZ181	Meitan	Mudstone	159.13	-25.31	0.12		
GZ32	Meitan	Carbonate	159.20	-26.72	0.05	-1.18	-10.27
GZ33	Meitan	Carbonate	159.91	-25.65	0.03	-1.15	-9.76
GZ34	Meitan	Carbonate	159.26	-24.72	0.05	-0.99	-9.79
GZ35	Meitan	Carbonate	160.84	-23.84	0.04	-0.89	-9.14
GZ36	Meitan	Carbonate	161.33	-23.26	0.02	-0.66	-8.51
GZ37	Meitan	Carbonate	162.42	-25.73	0.03	-1.18	-10.12
GZ182	Meitan	Mudstone	167.93	-25.04	0.11		
GZ183	Meitan	Mudstone	173.39	-25.34	0.11		
GZ184	Meitan	Mudstone	178.84	-25.66	0.21		
GZ185	Meitan	Mudstone	182.30	-27.98	0.31		
GZ186	Meitan	Mudstone	187.50	-23.08	0.04		
GZ41	Meitan	Carbonate	194.28	-24.34	0.03	-1.27	-10.19
GZ42	Meitan	Carbonate	195.37	-25.65	0.04	-1.25	-9.86
GZ187	Meitan	Mudstone	202.66	-24.37	0.08		
GZ44	Meitan	Carbonate	209.28	-25.25	0.04	-1.25	-10.26
GZ45	Meitan	Carbonate	209.82	-26.38	0.05	-1.79	-10.34
GZ188	Meitan	Mudstone	213.66	-26.95	0.18		
GZ189	Meitan	Mudstone	221.30	-26.84	0.17		
GZ190	Meitan	Mudstone	229.93	-27.21	0.25		
GZ191	Meitan	Mudstone	241.48	-26.54	0.19		
GZ193	Meitan	Mudstone	254.57	-25.40	0.12		
GZ194	Meitan	Mudstone	263.30	-25.25	0.10		
GZ47	Meitan	Carbonate	278.46	-25.34	0.05	-1.11	-8.75
GZ48	Meitan	Carbonate	281.73	-26.89	0.04	-0.73	-9.22
GZ196	Meitan	Mudstone	276.39	-27.99	0.07		
GZ197	Meitan	Mudstone	289.20	-28.58	0.10		
GZ49	Shihtzupu	Carbonate	292.15	-26.23	0.07	1.53	-8.48
GZ50	Shihtzupu	Carbonate	294.27	-26.58	0.06	1.39	-8.88
GZ51	Shihtzupu	Carbonate	294.95	-27.92	0.05	1.21	-8.76
GZ52	Shihtzupu	Carbonate	295.10	-27.51	0.09	0.80	-8.58

(continued on next page)

Table 1 (continued)

Sample	Formation	Lithology	Depth (m)	$\delta^{13}\text{C}_{\text{org}}$	Corg (%)	$\delta^{13}\text{C}_{\text{carb}}$	$\delta^{18}\text{O}_{\text{carb}}$
GZ53	Shihtzupu	Carbonate	295.25	-27.16	0.07	0.89	-8.33
GZ54	Shihtzupu	Carbonate	295.85	-27.32	0.08	0.92	-8.23
GZ55	Shihtzupu	Carbonate	296.31	-26.44	0.07	1.00	-8.67
GZ56	Shihtzupu	Carbonate	296.76	-27.37	0.08	0.96	-8.80
GZ57	Shihtzupu	Carbonate	297.52	-27.22	0.06	1.12	-8.90
GZ58	Shihtzupu	Carbonate	297.97	-26.87	0.05	0.96	-8.90
GZ59	Shihtzupu	Carbonate	298.73	-27.09	0.06	0.63	-8.90
GZ60	Shihtzupu	Carbonate	299.03	-26.89	0.04	0.90	-8.86
GZ61	Shihtzupu	Carbonate	299.94	-26.53	0.06	0.35	-8.79
GZ62	Shihtzupu	Carbonate	300.69	-26.38	0.05	0.50	-8.83
GZ63	Shihtzupu	Carbonate	301.45	-27.15	0.04	0.72	-8.89
GZ64	Pagoda	Carbonate	301.64	-29.82	0.10	0.85	-8.64
GZ65	Pagoda	Carbonate	303.50	-28.99	0.07	2.22	-8.40
GZ66	Pagoda	Carbonate	306.45	-26.07	0.02	2.14	-9.23
GZ67	Pagoda	Carbonate	309.10	-25.72	0.03	2.04	9.05
GZ68	Pagoda	Carbonate	313.44	-28.12	0.07	1.61	-9.15
GZ69	Pagoda	Carbonate	317.00	-29.81	0.11	1.55	-9.05
GZ70	Pagoda	Carbonate	321.00	-26.94	0.04	1.50	-9.02
GZ71	Pagoda	Carbonate	324.55	-26.99	0.02	1.56	-9.31
GZ72	Pagoda	Carbonate	328.66	-27.40	0.12	2.74	-9.19
GZ73	Pagoda	Carbonate	333.43	-29.02	0.10	1.99	-9.16
GZ74	Pagoda	Carbonate	337.35	-28.98	0.10	1.95	-9.22
GZ75	Linhsiang	Carbonate	338.55	-28.76	0.07	0.46	-9.65
GZ76	Linhsiang	Carbonate	339.05	-26.07	0.06	1.19	-9.37
GZ77	Linhsiang	Carbonate	341.65	-28.97	0.06	1.32	-9.31
GZ78	Linhsiang	Carbonate	342.15	-27.70	0.03	0.77	-9.48

However, it appears that the  $\delta^{13}\text{C}_{\text{carb}}$  values of the Pagoda carbonates decrease from +2.7‰ to +0.8‰ in the upper Katian (Fig. 5A).

#### 4.3. C-isotope excursions and global correlations

At Honghuayuan, a large (+8‰) excursion in  $\delta^{13}\text{C}_{\text{org}}$  is observed over a 75-m-thick stratigraphic interval in the lower to mid-Floian, from the *Acrograptus filiformis* through the *Didymograptus eobifidus* biozones of the Meitan Formation (Fig. 4B). The relatively smooth character of this excursion (as reflected in limited sample-to-sample variance) suggests that it represents a perturbation to the global carbon cycle rather than a response to local environmental factors or to post-depositional processes. This excursion may be correlative with C-isotopic excursions identified in age-equivalent sections elsewhere. In southwestern Argentina,  $\delta^{13}\text{C}_{\text{carb}}$  values rise from -2.8‰ to 0.3‰ from the *P. proteus* to the *O. evae* conodont biozones of the Arenigian, which is probably equivalent to the Floian (Buggisch et al., 2003) (Fig. 4C). Upward, the C-isotope data show a decreased trend towards the Early Darriwilian (Buggisch et al., 2003) (Fig. 4C). Within the correlative interval of the Argentinian section,  $\delta^{13}\text{C}$  values show a parallel increase of ~+2.8‰ (Buggisch et al., 2003). There is no  $\delta^{13}\text{C}_{\text{carb}}$  data for the lower to mid-Floian at Honghuayuan because of a lack of carbonate deposits. However, the correlative biostratigraphy based on conodont and graptolite biozones between South China and southwestern Argentina allow us to correlate the positive  $\delta^{13}\text{C}$  excursions observed from the two areas.

The positive increase of ~3‰ for  $\delta^{13}\text{C}_{\text{carb}}$  (i.e., -1‰ to +2‰) in the Darriwilian stage at Honghuayuan has been reported from elsewhere (Fig. 5A). For example, in central Nevada, a  $\delta^{13}\text{C}_{\text{carb}}$  increase from -2‰ to 0‰ was observed in the middle Chazy stage (Saltzman and Young, 2005). At Valga-Mehikoorma in Estonia,  $\delta^{13}\text{C}_{\text{carb}}$  values rise from -0.5‰ to +1.5‰ from the Kunda stage to the Aseri stage at, exhibiting a ~2‰ positive increase in mid-Darriwilian (Kaljo et al., 2007). Also, a positive excursion of ~1.5‰ for  $\delta^{13}\text{C}_{\text{carb}}$  was reported in the Darriwilian stage of southwestern Argentina (Buggisch et al., 2003). These C-isotopic data suggest that the the mid-Darriwilian carbon isotope excursion (Fig. 5) may be of global significance and provide evidence of a major perturbation to the global carbon cycle at that time.

Saltzman and Young (2005) observed positive C-isotopic excursions of 1–2‰ in the Turinian stage of the Mohawkian in Nevada (western United States) (Fig. 5B). The age of the boundary between the Turinian and Chatfieldian is 454 Ma (Ludvigson et al., 2004), which may be equivalent to the Sandbian stage. If so, the increase of ~2‰ for  $\delta^{13}\text{C}_{\text{carb}}$  in the lowermost Sandbian stage at Honghuayuan probably can be correlated to that in the Turinian stage in North America.

At Honghuayuan,  $\delta^{13}\text{C}_{\text{carb}}$  data show little apparent stratigraphic trend for the Pagoda Formation spanning lower Sandbian to Katian. A positive C-isotopic event of putative global extent, known as the Guttenberg Inorganic Carbon Excursions (GICE), had been reported for the early Katian (Fig. 5B). GICE has been observed from North America (Pancost et al., 1999; Saltzman and Young, 2005), Baltic (Kaljo et al., 2007), and from the Pagoda Formation in South China (Bergström et al., 2009). The apparent lack of GICE in the Honghuayuan section (Fig. 5A) may reflect possible preservation biases of the isotopic record at this locale.

#### 4.4. Implications of C-isotopic variation for the GOBE

Various explanations have been offered for C-isotopic excursions in the stratigraphic record, among which one of the most common interpretations of positive excursions is that they reflect increases in organic carbon burial rate that may be associated with concurrent decreases in atmospheric  $\text{pCO}_2$  (Arthur et al., 1988; Patzkowsky et al., 1997; Kump and Arthur, 1999). Because photosynthesis fractionate in favor of  $^{12}\text{C}$  relative to the source of inorganic carbon (by ~20‰ to 25‰ for plants using the Hatch–Slack photosynthetic cycle), higher rates of primary productivity probably driven by increased availability of nutrients and subsequent burial of  $^{12}\text{C}$ -enriched organic matter cause the dissolved inorganic carbon (DIC) reservoir in seawater to become enriched in  $^{13}\text{C}$ . Based on these relationships, concurrent large positive C-isotopic excursions in the mid-Floian of South China and southwestern Argentina (Fig. 4B–C) are inferred to be indicative of a major organic carbon burial event and a probable simultaneous decrease in atmospheric  $\text{pCO}_2$  during the Early Ordovician (cf. Saltzman, 2005).

Paleontologic studies of the Early Ordovician radiation in South China have documented a rapid diversification commencing in the

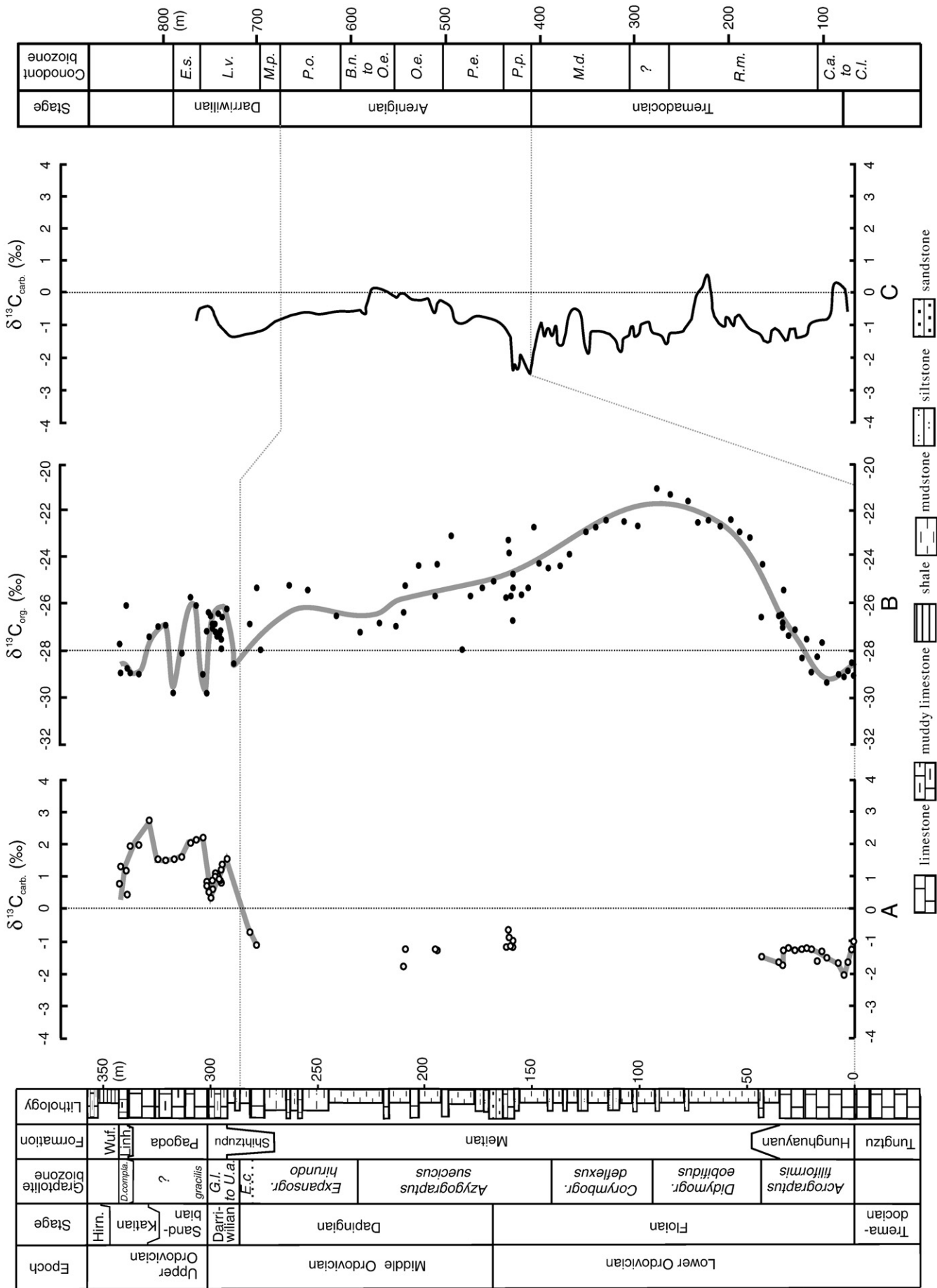


Fig. 4. C-isotopic chemostratigraphy of the Honghuayuan section in South China and its correlation to that in Argentina. (A)  $\delta^{13}C_{carb}$ , (B)  $\delta^{13}C_{org}$ , and (C) correlation to  $\delta^{13}C_{carb}$ . (B)  $\delta^{13}C_{org}$  and (C) correlation to  $\delta^{13}C_{carb}$ . (A)  $\delta^{13}C_{carb}$  profile for southwestern Argentina (Bugghisch et al., 2003). Graptolite taxonomic abbreviations: *D. compla.* = *Dicellograptus complanatus*, *E.c.* = *Exigraptus clavus*, *G.l.* = *Gymnograptus linnarssoni*, *U.a.* = *Undulograptus austrodenatus*. Conodont taxonomic abbreviations: *B.n.* = *B. navis*, *C.a.* = *C. angulatus*, *C.i.* = *C. lindstromi*, *E.s.* = *E. suecicus*, *L.v.* = *L. variabilis*, *M.d.* = *Macerodus diana*, *M.p.* = *M. parva*, *O.e.* = *O. evae*, *P.o.* = *P. originalis*, *P.e.* = *P. elegans*, *P.p.* = *P. proteus*, *R.m.* = *R. mantouensis*.

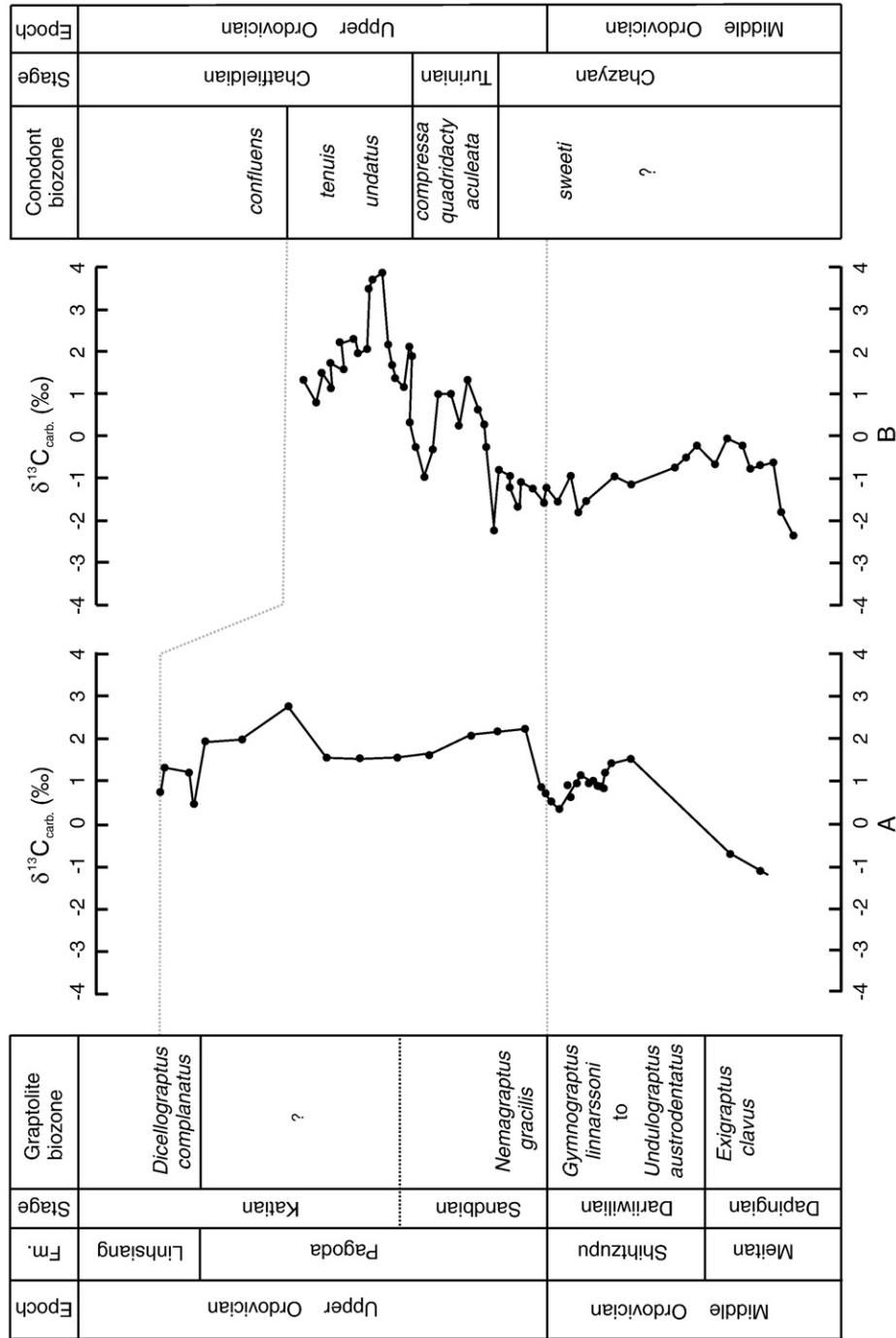


Fig. 5. Detailed C-isotopic chemostratigraphy of Middle to Upper Ordovician interval at Honghuayuan: (A)  $\delta^{13}\text{C}_{\text{carb}}$ ; and (B) correlation to  $\delta^{13}\text{C}_{\text{carb}}$  profile for Nevada (Saltzman and Young, 2005).

*Acrograptus filiformis* biozone at the base of the Meitan Formation and reaching the first peak at the top of the *Didymograptus eobifidus* biozone (Fig. 2). Thus, the beginning of the diversification event was concurrent with the onset of the extended +8‰ excursion in  $\delta^{13}\text{C}_{\text{org}}$  in the Floian stage at Honghuayuan (Fig. 4B). Based on relationships between the  $\delta^{13}\text{C}$  of seawater DIC and atmospheric  $\text{pCO}_2$  discussed above, this excursion provides evidence of probable strong climatic cooling during the Early Ordovician that may have been an important factor in the GOBE (c.f. Trotter et al., 2008).

At Honghuayuan, the  $\delta^{13}\text{C}_{\text{carb}}$  record exhibits episodic increases within the middle Darriwilian and basal Sandbian (Fig. 4A). These  $\delta^{13}\text{C}_{\text{carb}}$  increases suggest that enhanced burial rates of organic matter continued to occur episodically during the late Middle and early Late Ordovician. Such episodes of enhanced organic carbon burial are likely to have led to further declines in atmospheric  $\text{pCO}_2$  and global climatic cooling. This interpretation is consistent with the results of an oxygen-isotopic thermometry study of contemporaneous conodonts, which documented a probable decrease in global temperatures from 42 °C in the early Tremadocian to 28 °C in the middle Darriwilian (Trotter et al., 2008). We suggest that episodes of enhanced organic carbon burial, as evidenced by C-isotopic increases observed at Honghuayuan (Fig. 4), may have been an important factor in contributing to the late Middle and early Late Ordovician cooling trend that culminated in the Hirnantian glaciation.

## 5. Conclusions

High-resolution organic carbon and carbonate carbon isotopic records from a well-exposed section at Honghuayuan in South China provide one of the most complete records through the Ordovician. These records reveal large perturbations that can be correlated with C-isotopic records from other basins and, hence, may be indicative of perturbations to the global carbon cycle. The episodic increases in  $\delta^{13}\text{C}_{\text{org}}$  and  $\delta^{13}\text{C}_{\text{carb}}$  values observed at Honghuayuan in South China suggest enhanced burial rates of organic matter during the Early to early Late Ordovician. Climatic cooling as a consequence of enhanced organic carbon burial is likely to have been an important role in triggering both the GOBE and the end-Ordovician mass extinction. Although biodiversification may have been promoted during the Early to Middle Ordovician by climatic cooling, intensified cooling during the Late Ordovician had a harmful effect on contemporaneous marine biotas.

## Acknowledgments

We thank Renbin Zhan for help in the field work. We thank Peter Sheehan and Jesper Nielsen and an anonymous reviewer for constructive comments. This study was supported by National Natural Science Foundation of China (40528004, 40503002). TJA acknowledges support from the National Science Foundation.

## References

Algeo, T.J., Wilkinson, B.H., Lohmann, K.C., 1992. Meteoric-burial diagenesis of Pennsylvanian carbonate: water/rock interactions and basin geothermics. *J. Sediment. Petrol.* 62, 652–670.

Arthur, M.A., Dean, W.E., Pratt, L.M., 1988. Geochemical and climatic effects of increased marine organic carbon burial at the Cenomanian/Turonian boundary. *Nature* 335, 714–717.

Berner, R.A., Kothavala, Z., 2001. GEOCARB III: a revised model of atmospheric  $\text{CO}_2$  over Phanerozoic time. *Am. J. Sci.* 301, 182–204.

Bergström, S.M., Chen, X., Schmitz, B., Young, S., Rong, J., Saltzman, M.R., 2009. First documentation of the Ordovician Guttenberg  $\delta^{13}\text{C}$  excursion (GICE) in Asia: chemostratigraphy of the Pagoda and Yanwashan formations in southeastern China. *Geol. Mag.* 146, 1–11.

Bottjer, D.J., Droser, M.L., Sheehan, P.M., McGhee Jr., G.R., 2001. The ecological architecture of major events in the Phanerozoic history of marine life. In: Allmon, W.D., Bottjer, D.J. (Eds.), *Evolutionary Paleocology: The Ecological Context of Macroevolutionary Change*. Columbia Univ. Press, pp. 35–61.

Brenchley, P.J., Carden, G.A., Hints, O., Kaljo, D., Marshall, J.D., Martma, T., Meidla, T., Nolvak, J., 2003. High-resolution stable isotope stratigraphy of Upper Ordovician

sequences: constraints on the timing of bioevents and environmental changes associated with mass extinction and glaciation. *Geol. Soc. Am. Bull.* 115, 89–104.

Buggisch, W., Keller, M., Lehnert, O., 2003. Carbon isotope record of Late Cambrian to Early Ordovician carbonates of the Argentine Precordillera. *Palaeogeogr. Palaeoclimatol. Palaeoecol.* 195, 357–373.

Chen, X., Rong, J., Wang, X., Wang, Z., Zhang, Y., Zhan, R., 1995. Correlation of Ordovician Rocks of China, 31. International Union of Geol. Sci. Publ. 104 pp.

Chen, X., Rong, J., Mitchell, C.E., Harper, D.A.T., Fan, J., Zhan, R., Zhang, Y., Li, R., Wang, Y., 2000. Late Ordovician to earliest Silurian graptolite and brachiopod zonation from Yangtze Region, South China with global correlation. *Geol. Mag.* 137, 623–650.

Chen, X., Rong, J., Li, Y., Boucot, A.J., 2004. Facies patterns and geography of the Yangtze region, South China, through the Ordovician and Silurian transition. *Palaeogeogr. Palaeoclimatol. Palaeoecol.* 204, 353–372.

Chen, X., Melchin, M.J., Sheets, H.D., Mitchell, C.E., Fan, J.X., 2005. Patterns and processes of latest Ordovician graptolite extinction and recovery based on data from south China. *J. Paleontol.* 79, 842–861.

Chen, X., Rong, J., Fan, J., Zhan, R., Mitchell, C., Harper, D.A.T., Melchin, M.J., Peng, P., Finney, S.C., Wang, X., 2006a. The global boundary stratotype section and point for the base of the Hirnantian Stage (the uppermost of the Ordovician System). *Episodes* 29, 183–196.

Chen, X., Zhang, Y., Fan, J., 2006b. Ordovician graptolite evolutionary radiation: a review. *Geol. J.* 41, 289–301.

Cramer, B.D., Saltzman, M.R., 2007. Early Silurian paired analyses from the Midcontinent of North America: implications for paleoceanography and paleoclimate. *Palaeogeogr. Palaeoclimatol. Palaeoecol.* 256, 195–203.

Crowell, J.C., 1999. Pre-Mesozoic Ice Ages: their bearing on understanding the climate system. *Geol. Soc. Am. Memoir.* 192, 106 pp.

Droser, M.L., Sheehan, P.M., 1997. Palaeoecology of the Ordovician Radiation; resolution of large-scale patterns with individual clade histories, palaeogeography and environments. *Geobios* 20, 221–229.

Fan, J., Peng, P., Melchin, M.J., 2009. Carbon isotopes and event stratigraphy near the Ordovician–Silurian boundary, Yichang, South China. *Palaeogeogr. Palaeoclimatol. Palaeoecol.* 276, 160–169.

Finney, S.C., Berry, W.B.N., Cooper, J.D., Ripperdan, R.L., Sweet, W.C., 1999. Late Ordovician mass extinction: a new perspective from stratigraphic sections in central Nevada. *Geology* 27, 215–218.

Freeman, K.H., 2001. Isotopic biogeochemistry of marine organic carbon. *Rev. Mineral. Geochem.* 43, 579–605.

Fu, K., 1982. The Ordovician of the Yangtze region. In: Lai, C. (Ed.), *The Ordovician System of China*. Stratigraphy of China 5. Geol. Publ. House, Beijing, pp. 92–131.

Gibbs, M.T., Barron, E.J., Kump, L.R., 1997. An atmospheric  $\text{pCO}_2$  threshold for glaciation in the Late Ordovician. *Geology* 27, 447–450.

Gradstein, F., Ogg, J., Smith, A., 2004. *A Geologic Time Scale*. Cambridge Univ. Press, 589 pp.

Hayes, J.M., Popp, B.N., Takigiku, R., Johnson, M.W., 1989. An isotopic study of biogeochemical relationships between carbonates and organic carbon on the Greenhorn Formation. *Geochim. Cosmochim. Acta* 68, 4363–4379.

Hayes, J.M., Strauss, H., Kaufman, A.J., 1999. The abundance of  $^{13}\text{C}$  in marine organic matter and isotopic fractionation in the global biogeochemical cycle of carbon during the past 800 Ma. *Chem. Geol.* 161, 103–125.

Herrmann, A.D., Patzkowsky, M.E., Pollard, D., 2003. Obliquity forcing with 8–12 times preindustrial levels of atmospheric  $\text{pCO}_2$  during the Late Ordovician glaciation. *Geology* 31, 485–488.

Hu, Y.H., Zhou, J.B., Song, B., Li, W., Sun, W.D., 2008. SHRIMP zircon U–Pb dating from K-bentonite in the top of Ordovician of Wangjiawan Section, Yichang, Hubei, China. *Sci. China Earth Sci.* 38, 72–77.

Ingalls, A.E., Aller, R.C., Lee, C., Wakeham, S.G., 2004. Organic matter diagenesis in shallow water carbonate sediments. *Geochim. Cosmochim. Acta* 68, 4363–4379.

Kaljo, D., Martma, T., Saadre, T., 2007. Post-Hunnebergian Ordovician carbon isotope trend in Baltoscandia, its environmental implications and some similarities with that of Nevada. *Palaeogeogr. Palaeoclimatol. Palaeoecol.* 245, 138–155.

Kump, L.R., Arthur, M.A., 1999. Interpreting carbon-isotope excursions: carbonates and organic matter. *Chem. Geol.* 161, 181–198.

Kump, L.R., Arthur, M.A., Patzkowsky, M.E., Gibbs, M.T., Pinkus, D.S., Sheehan, P.M., 1999. A weathering hypothesis for glaciation at high atmospheric  $\text{pCO}_2$  during the Late Ordovician. *Palaeogeogr. Palaeoclimatol. Palaeoecol.* 152, 173–187.

Lohmann, K.C., Walker, J.C.G., 1989. The  $\delta^{18}\text{O}$  record of Phanerozoic abiotic marine calcite cements. *Geophys. Res. Lett.* 16, 319–322.

Ludvigson, G.A., Witzke, B.J., Gonzalez, L.A., Carpenter, S.J., Schneider, C.L., Hasiuk, F., 2004. Late Ordovician (Turinian–Chatfieldian) carbon isotope excursions and their stratigraphic and paleoceanographic significance. *Palaeogeogr. Palaeoclimatol. Palaeoecol.* 210, 187–214.

Melchin, M.J., Holmden, C., 2006. Carbon isotope chemostratigraphy in Arctic Canada: Sea-level forcing of carbonate platform weathering and implications for Hirnantian global correlation. *Palaeogeogr. Palaeoclimatol. Palaeoecol.* 234, 186–200.

Miller, A.I., 1997. Dissecting global diversity trends: examples from the Ordovician radiation. *Annu. Rev. Ecol. System.* 28, 85–104.

Mu, E., Li, J., Ge, M., Chen, X., Ni, Y., Lin, Y., 1981. Late Ordovician paleogeography of South China. *Acta Stratigraphica Sinica* 5, 165–170.

Pancost, R.D., Freeman, K.H., Patzkowsky, M.E., 1999. Organic-matter source variation and the expression of a late Middle Ordovician carbon isotope excursion. *Geology* 27, 1015–1018.

Patzkowsky, M.E., Slupik, L.M., Arthur, M.A., Pancost, R.D., Freeman, K.H., 1997. Late Middle Ordovician environmental change and extinction: Harbinger of the Late Ordovician or continuation of Cambrian patterns? *Geology* 25, 911–914.

Rong, J., Chen, X., Harper, D.A.T., 2002. The latest Ordovician Hirnantia Fauna (Brachiopoda) in time and space. *Lethaia* 35, 231–249.

Rong, J., Harper, D.A.T., 1988. A global synthesis of the latest Ordovician Hirnantian brachiopod faunas. *Trans. Roy. Soc. Edinburgh (Earth Sci.)* 79, 383–402.

- Rong, J., Zhan, R., Harper, D.A.T., 1999. Late Ordovician (Caradoc–Ashgill) brachiopod faunas with *Foliomena* based on data from China. *Palaios* 14, 412–431.
- Royer, D.L., 2006. CO<sub>2</sub>-forced climate thresholds during the Phanerozoic. *Geochim. Cosmochim. Acta* 70, 5665–5675.
- Saltzman, M.R., 2005. Phosphorus, nitrogen, and the redox evolution of the Paleozoic oceans. *Geology* 33, 573–576.
- Saltzman, M.R., Young, S.A., 2005. Long-lived glaciation in the Late Ordovician? Isotopic and sequence-stratigraphic evidence from western Laurentia. *Geology* 33, 109–112.
- Schmitz, B., Harper, D.A.T., Peucker-Ehrenbrink, B., Stouge, S., Alwmark, C., Cronholm, A., Bergstrom, S.M., Tassinari, M., Wang, X., 2008. Asteroid breakup linked to the Great Ordovician Biodiversification Event. *Nature Geosci.* 1, 49–53.
- Selden, P.A., Edwards, D., 1989. Colonisation of the land. In: Allen, K., Briggs, D. (Eds.), *Evolution and the Fossil Record*. Belhaven, London, pp. 122–152.
- Sepkoski, J.J., 1996. Patterns of Phanerozoic extinction: a perspective from global data bases. In: Walliser, O.H. (Ed.), *Global Events and Event Stratigraphy in the Phanerozoic*. Springer, Berlin, pp. 35–51.
- Sepkoski, J.J., 1997. Biodiversity: past, present and future. *J. Paleontol.* 71, 533–539.
- Servais, T., Harper, D.A.T., Li, J., Munnecke, A., Owen, A.W., Sheehan, P.M., 2009. Understanding the Great Ordovician Biodiversification Event (GOBE): influences of paleogeography, paleoclimate, or paleoecology? *GSA Today* 19, 4–10.
- Sheehan, P.M., 2001. The Late Ordovician mass extinction. *Annu. Rev. Earth Planet. Sci.* 29, 331–364.
- Shen, Y., Schidlowski, M., 2000. New C isotope stratigraphy from southwest China: Implications for the placement of the Precambrian–Cambrian boundary on the Yangtze Platform and global correlations. *Geology* 28, 623–626.
- Shields, G.A., Garden, G.A.F., Veizer, J., Meidla, T., Rong, J., Li, R., 2003. Sr, C, and O isotope geochemistry of Ordovician brachiopods: a major isotope event around the Middle–Late Ordovician transition. *Geochim. Cosmochim. Acta* 67, 2005–2025.
- Stanley, S.M., 1984. Temperature and biotic crises in the marine realm. *Geology* 12, 205–208.
- Trotter, J.A., Williams, I.S., Barnes, C.R., Lecuyer, C., Nicoll, R.S., 2008. Did cooling oceans trigger Ordovician biodiversification? Evidence from conodont thermometry. *Science* 321, 550–554.
- Underwood, C.J., Crowley, S.F., Marshall, J.D., Brenchley, P.J., 1997. High-resolution carbon isotope stratigraphy of the basal Silurian stratotype (Dob's Linn, Scotland) and its global correlation. *J. Geol. Soc. Lond.* 154, 709–718.
- Wang, H., 1985. *Atlas of the Paleogeography of China*. Cartographic Publ, House, Beijing, 143 pp.
- Wang, H., Chen, J., 1991. Late Ordovician and early Silurian rugose coral biogeography and world reconstruction of palaeocontinents. *Palaeogeogr. Palaeoclimatol. Palaeoecol.* 86, 3–21.
- Wang, K., Orth, C.J., Attrep, M., Chatterton, B.D.E., Wang, X., Li, J., 1993a. The great latest Ordovician extinction on the South China Plate: chemostratigraphic studies of the Ordovician–Silurian boundary interval on the Yangtze platform. *Palaeogeogr. Palaeoclimatol. Palaeoecol.* 104, 61–79.
- Wang, K., Chatterton, B.D.E., Attrep, M., Orth, C.J., 1993b. Late Ordovician mass extinction in the Selwyn Basin, northwestern Canada. *Can. J. Earth Sci.* 30, 1870–1880.
- Wang, K., Chatterton, B.D.E., Wang, Y., 1997. An organic carbon isotope record of Late Ordovician to Early Silurian marine sedimentary rocks, Yangtze Sea, South China: implications for CO<sub>2</sub> changes during the Hirnantian glaciation. *Palaeogeogr. Palaeoclimatol. Palaeoecol.* 132, 147–158.
- Wang, X., Hoffknecht, A., Xiao, J., Chen, S., Li, Z., Broche, R.B., Erdtmann, B.D., 1993c. Graptolite, chitinozoan and scolecodont reflectances and their use as indicators of thermal maturity. *Acta Geol. Sinica* 6, 93–105.
- Webby, B.D., Paris, F., Droser, M.L., 2004. *The Great Ordovician Biodiversification Event*. Columbia Univ. Press, New York, 484 pp.
- Yan, D., Chen, D., Wang, Q., Wang, J., Wang, Z., 2009. Carbon and sulfur isotopic anomalies across the Ordovician–Silurian boundary on the Yangtze Platform, South China. *Palaeogeogr. Palaeoclimatol. Palaeoecol.* 274, 32–39.
- Zhan, R., Rong, J., Cheng, J., Chen, P., 2005. Early–Mid Ordovician brachiopod diversification in South China. *Sci. China Earth Sci.* 48, 662–675.
- Zhan, R., Harper, D.A.T., 2006. Biotic diachroneity during the Ordovician radiation: evidence from South China. *Lethaia* 39, 211–226.
- Zhan, R., Jin, J., 2007. Ordovician–Early Silurian (Llandovery) stratigraphy and palaeontology of the Upper Yangtze Platform. South China, Science Press, Beijing, 169 pp.
- Zhan, R., Jin, J., 2008. Aspects of recent advances in the Ordovician stratigraphy and palaeontology of China. *Paleoworld* 17, 1–11.
- Zhan, R., Jin, J., Chen, P., 2007. Brachiopod diversification during the Early–Middle Ordovician: an example from Dawan Formation, Yichang, central China. *Can. J. Earth Sci.* 44, 9–24.
- Zhang, T., Shen, Y., Zhan, R., Shen, S., Chen, X., 2009. Large perturbations of the carbon and sulfur cycle associated with the Late Ordovician mass extinction in South China. *Geology* 37, 299–302.
- Zhang, Y., Chen, X., 2003. The Early Ordovician graptolite sequence of the Upper Yangtze region, South China. *INSUGEO Serie Correlacion Geologia* 17, 173–180.